energies

MDPI

Article

A Micro-Nuclear Power Generator for Space Missions

Olukayode L. Ayodele *, Doudou N. Luta * and Mohammed T. Kahn *

Department of Mechanical and Mechatronic Engineering, Cape Peninsula University of Technology, Cape Town 7530, South Africa

* Correspondence: ayodeleo@cput.ac.za (O.L.A.); lutad@cput.ac.za (D.N.L.); khant@cput.ac.za (M.T.K.)

Abstract: The significance of reliable energy storage systems in spacecraft applications cannot be overstated, since they play a vital role in ensuring continuous power supply and prolonged mission durations. This research deals with the modeling of a hybrid multi-mission radioisotope thermoelectric generator (MMRTG)-lithium-ion (Li-ion) battery integrated energy storage system for spacecraft applications to combine the RTGs' long lifespan and reliability benefits alongside the Li-ion battery's rechargeability and high energy density to achieve a single energy unit. The investigation's main problem was exploring a power unit that improves the limitations of MMRTG and Li-ion batteries to achieve a highly efficient and reliable power supply for autonomous systems, such as a spacecraft. The proposed hybrid system comprises a 110 W/32 V RTG and a 3.6 V/43 Ah Li-ion battery connected to a DC motor through power converters. Results demonstrate the potential of the adopted hybrid energy system in improving the efficiency, reliability, and mission duration of spacecraft missions. The assessment of the hybrid energy system under various load conditions shows that the highest power peak of 3500 W was achieved at a load resistance of 1 Ω. Furthermore, the results show that the hybrid energy system output voltage at temperatures of 253 °K and 293 °K are relatively equal. However, the power cycle was wider and required a long time before dropping.

Keywords: RTG; MMRTG; Li-ion battery; spacecraft; energy storage

Citation: Ayodele, O.L.; Luta, D.N.; Kahn, M.T. A Micro-Nuclear Power Generator for Space Missions. *Energies* **2023**, *16*, 4422. https://doi.org/10.3390/en16114422

Academic Editors: Mikołaj Oettingen, Paweł Gajda and Bartosz Ceran

Received: 26 April 2023
Revised: 23 May 2023
Accepted: 29 May 2023
Published: 30 May 2023

1. Introduction

The growing interest in earth monitoring, satellite activity, space exploration, and structural health monitoring in extreme and inaccessible environments has increased the demand for power sources for autonomous systems. Autonomous systems are designed to operate in known or unfamiliar environments for as long as possible for processing, providing, and storing data without being connected to an electrical grid. Without human intervention, the system may operate in an external natural or industrial environment for long periods.

Autonomous space exploration missions might require several years before accomplishing the objectives they were sent to perform, yet they, nevertheless, remain continuously powered. This is to ensure the control of navigation and communication; therefore, it is necessary to have a long-life power source accompanied by an energy storage unit capable of storing the excess energy. Moreover, a single power source system usually must feed or absorb power peaks to or from the load; this mixed operation can be disadvantageous, resulting in an overweight energy source with a shorter lifespan. Furthermore, some situations might require additional power. Meanwhile, a single source system only provides average power, ensuring the primary function of the spacecraft.

Batteries in spacecrafts have been mainly used for load leveling and supplying considerable power for some time. Such situations can be solved by adding a rechargeable battery to provide power during high demands [1,2]. Thus, combining an electrochemical battery with a radioisotope thermoelectric energy source to create a hybrid power source would result in a highly efficient and reliable energy source.

Radioisotope thermoelectric generators (RTGs) (Figure 1) are increasingly being used in space mission power systems [3,4]. RTGs are nuclear power generators that generate energy from radionuclide spontaneous decay, as opposed to nuclear fission energy from reactor power systems [5]. Electrical power systems can be affected by radiation in several ways; high radiant energy, including gamma rays, has the potential to weaken insulation and impact the performance of electrical systems. It may result in higher failure rates, decreased system reliability, and adverse effects on worker safety. Electrical power systems are shielded from radiation sources outside the system using shielding techniques. Additionally, radiation-tolerant materials can be used in system designs to improve resilience and lessen the impact of radiation on electrical power [6]. Radiation damage studies on structural materials can help you understand how a material behaves in a nuclear power unit. Oxide dispersion-strengthened steel alloys are potential radiation-tolerant materials, especially for high-temperature applications in nuclear power generation [7,8].

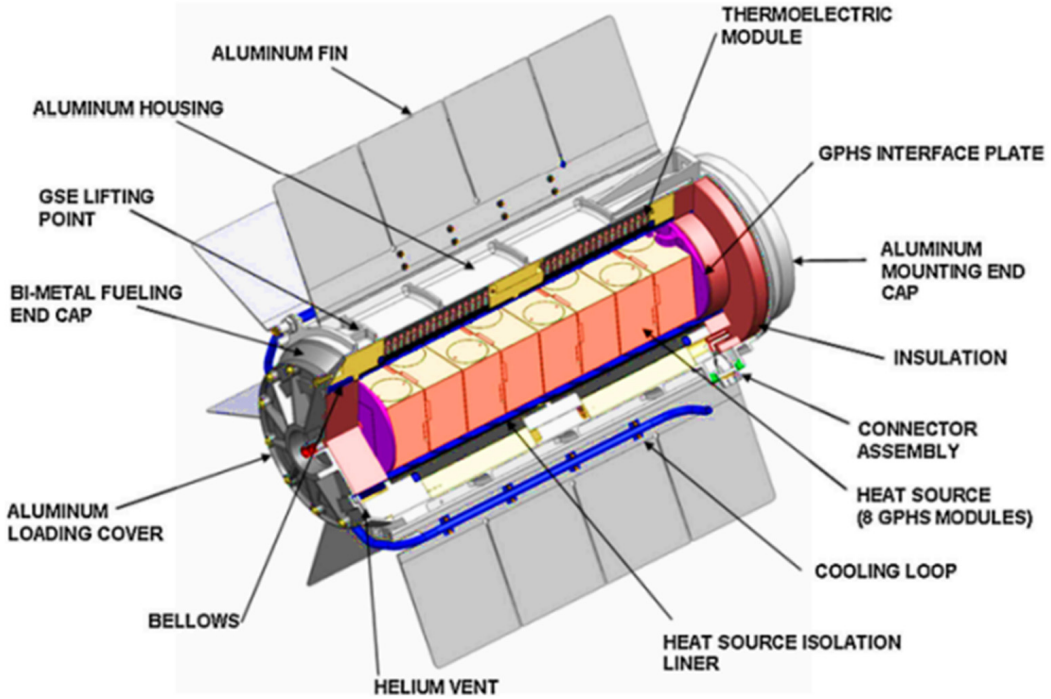

Figure 1. Multi-mission radioisotope thermal generator [5].

However, alpha and beta emitters are the most used radioisotopes since they do not necessitate as much shielding as gamma emitters. The main elements of such power units are a radioisotope heat source and an energy conversion system. Within the heat source, heat escapes during the decay process. This heat can be used by radioisotope thermoelectric generators (RTGs) to produce hundreds of Watts of electrical power through either a static or dynamic energy conversion mechanism employing the Seebeck effect [9], and the waste heat is dissipated into space or the surrounding areas. The military [10], gas and heat sensors [11], remote telephony, navigation, and instrument protection are some fields where RTGs have found their use [12].

The United States National Aeronautics and Space Administration (NASA) initially developed the general-purpose heat source-radioisotope thermoelectric generators (GPHS-RTGs) [13], and in support of NASA, the US Department of Energy (DOE) developed the multi-mission radioisotope thermoelectric generators (MMRTGs) [14]. The advantages of MMRTGs include a longer life, a higher power density, and a lower weight when compared to other power sources, such as solar energy. They also perform well in adverse weather conditions, varying temperatures and pressures, dense atmospheres, and vacuums. As a result, their applications are becoming more diverse.

In general, thermoelectric generator advantages include the absence of toxic residuals, compact, extremely reliable, simple, independent of position, scalable, running silently, and practically maintenance-free [15]. Sethumadhavan and Burger stated that [16] despite the merits above, a thermoelectric generator exhibits a relatively low efficiency, typically less than 10%. This drawback has limited its application to specialized military, medical, and aerospace missions, including radioisotope power for deep space probes and remote power such as oil pipelines and sea buoys, whereby safety and reliability are more important than cost. Since the sources of heat for a thermoelectric generator are almost free, as in the case of waste heat, where the comparatively low efficiency of the thermoelectric generation is not an overriding consideration, the running cost of a thermoelectric generator compensates for the relatively high construction costs [17].

Jaziri et al. [18] state that the isotope used for radioisotope thermoelectric generators (RTGs) as primary energy sources must exhibit characteristics such as low radiation emission, acceptable fuel half-life with the mission duration, high melting point, high power density, and safety in all conditions. Table 1 provides the characteristics of the most common isotope materials for RTGs. Of these isotope materials, Ce-144, Po-210, Sr-90, and Pm-147 exhibited significant limitations during testing, while Ce-144 had a half-life of 285 days, which was only suitable for a 6-month space mission [19].

Table 1. Characteristics of isotope materials used to generate electricity for spacecraft [20].

Isotope	Main Modes of Radiation Emissions	Half-Life	Melting Point °C	Specific Power Watts (th)/gm
Po-210	Alpha and few Gamma	136.38 days	254	31.7
Am-241	Alpha and Gamma	432.2 years	1176	0.11
Pm-147	Beta and few Gamma	2.6234 years	2375	0.33
Sr-90	Beta	29 years	770	0.93
Pu-238	Alpha and Gamma	87.74 years	640	0.56
Ce-144	Beta and Gamma	284.4 days	800	25.6

Of all these isotope materials, the Pu-238 stands as the most appropriate isotope fuel despite its high price. It has a high melting point, low gamma radiation, and a long half-life of 89.6 years, allowing it to be used in long-term missions without a power-fluttering device. Jaziri et al. [18] assert that since 1961, the DOE and US space missions have focused on developing the Pu-238 for use in space programs.

On the other hand, the choice of Li-ion battery over other electrochemical batteries, such as lead-acid, NiCd, and NiMH, is because of their relative advantages, whereby Li-ion batteries provide significant weight and volume benefits, good low-temperature performance, low self-discharge, high energy density, and high efficiency compared to other electrochemical batteries [21–23]. The current Li-ion batteries used for most of the NASA-JPL missions were developed by a NASA consortium, including Yardney Technical Products (YTP) and Jet Propulsion Laboratory (JPL) [24].

Currently, two different kinds of Li-ion batteries are used: those built with small-capacity cylindrical Li-ion cells and those made with large-capacity prismatic or cylindrical Li-ion cells [25]. Large-capacity prismatic Li-ion cell batteries were a key enabler in the Mars Exploration Rover (MER) missions [26].

The excellent performance of the MER mission in 2003 encouraged NASA to further the development of a new battery for their Mars Science Laboratory (MSL) mission in 2011. The "Curiosity" rover landed on Mars on 6 August 2012, to study the planet's ability to support microbial life that because of the requirements of the mission necessity lasted 687 Martian Solar days instead of the 90 in previous missions. The battery used in the mission was two 8-cell strings of 43 Ah prismatic cells which were manufactured by the Yardney Division at EaglePicher. Similarly, extensive ground testing was conducted on the battery cells under various conditions, including charge-discharge cycle rate testing,

life cycle estimation under extensive full discharge, and battery simulation under Mars surface operation.

The disadvantages of Li-ion batteries outweigh their benefits since they have low specific energies (100–265 Wh per kg) and poor energy densities (250–670 Wh per L). Other drawbacks of Li-ion batteries include their poor abuse tolerance (during accidental overcharge/over-discharge and short circuit as well as incompatibility with conventional planetary protection techniques), limited resilience to high-temperature exposure (>60 °C), limited low-temperature operational capability (<−30 °C), and limited resilience to low-temperature exposure [27].

Innovative methods for energy conversion into valuable forms can considerably enhance the growth of sustainable energy sources and satisfy the increasing demand for electricity in space applications. Compact power units with a high-power density and a long lifetime are necessary to operate space systems.

The underlined merit of this research is that it will provide a ground for alternative power to electrochemical batteries, fuel cells, and solar and wind energy sources with inherent limitations. Electrical energy derivable from radioisotopes has an energy density that can be about a hundred times higher than electrochemical batteries and ten times higher than hydrogen-based fuel cell fuels. Based on the spontaneous decay of readily available radioisotopes, micronuclear generators will produce a completely 'green' energy that is reliable and cheaper to operate and maintain. The possibility of having the radioisotope-based power source on a microscale will be a breakthrough for autonomous systems that can function over a considerable lifespan. Furthermore, combining an electrochemical battery with a radioisotope thermoelectric energy source to form a hybrid power source would create a highly efficient and reliable energy source.

This investigation's main problem was exploring a power unit that improved the limitations of MMRTG and Li-ion batteries to achieve a highly efficient and reliable power supply with an increased lifespan for autonomous systems, such as a spacecraft.

Thus, this study aimed to model and simulate a hybrid energy storage system combining electrochemical and nuclear batteries. The modeling and simulation were carried out using Matlab/Simulink environments. The study's specific objectives included developing the Simulink of the integrated energy storage combining electrochemical and nuclear batteries and auxiliary components and assessing the effect of temperature on the hybrid battery system.

The upcoming sections of the paper are organized as follows: Section 2 outlines the research design adopted in this study; Section 3 analyzes the simulation results; Section 4 summarizes the findings by making relevant contributions to the research problem investigation and recommendations for future research.

2. Research Design

To achieve the objectives of the investigation, the following steps were adopted in the research design:

- Identify and gather technical specifications for the MMRTG and Li-ion battery to be integrated to determine the electrical characteristics, power output, and capacity of the MMRTG and Li-ion battery.
- Develop mathematical models for the MMRTG and Li-ion battery based on their electrical characteristics and performance parameters, incorporate appropriate equations to represent the heat generation and energy conversion processes in the MMRTG, and use established models for Li-ion batteries considering the battery internal resistance, charge, and discharge rates and voltage–current characteristics.
- Establish a MATLAB model that integrates the MMRTG and Li-ion battery systems, define the power flow between the MMRTG and battery accounting for the charging and discharging processes, and incorporate control algorithms of the power converters to manage the power transfer, and optimize system performance.

- Simulate and analyze the simulation results to evaluate the performance of the developed hybrid system and compare the performance of the hybrid system with standalone MMRTG and Li-ion battery to determine the limitations and benefits of the integration.

2.1. Adopted System Description

The adopted hybrid system shown in Figure 2 combines a multi-mission radioisotope thermoelectric generator (MMRTG), an electrochemical battery (Li-ion), and complementary components, including a DC-DC boost converter, a half-bridge converter, and a load. The MMRTG has an electrical power capacity of 110 W at 32 V, whereas its thermal power is 2000 W. The MMRTG is connected to the load through a DC/DC converter controlled using a maximum power tracking algorithm to convert the MMRTG voltage to 60 V. The Li-ion battery, on the other hand, has a capacity of 43 Ah and operates at a voltage of 3.6 V. The battery is connected to the spacecraft load through a bidirectional converter, which provides 60 V to the battery, while also allowing the battery to charge whenever required.

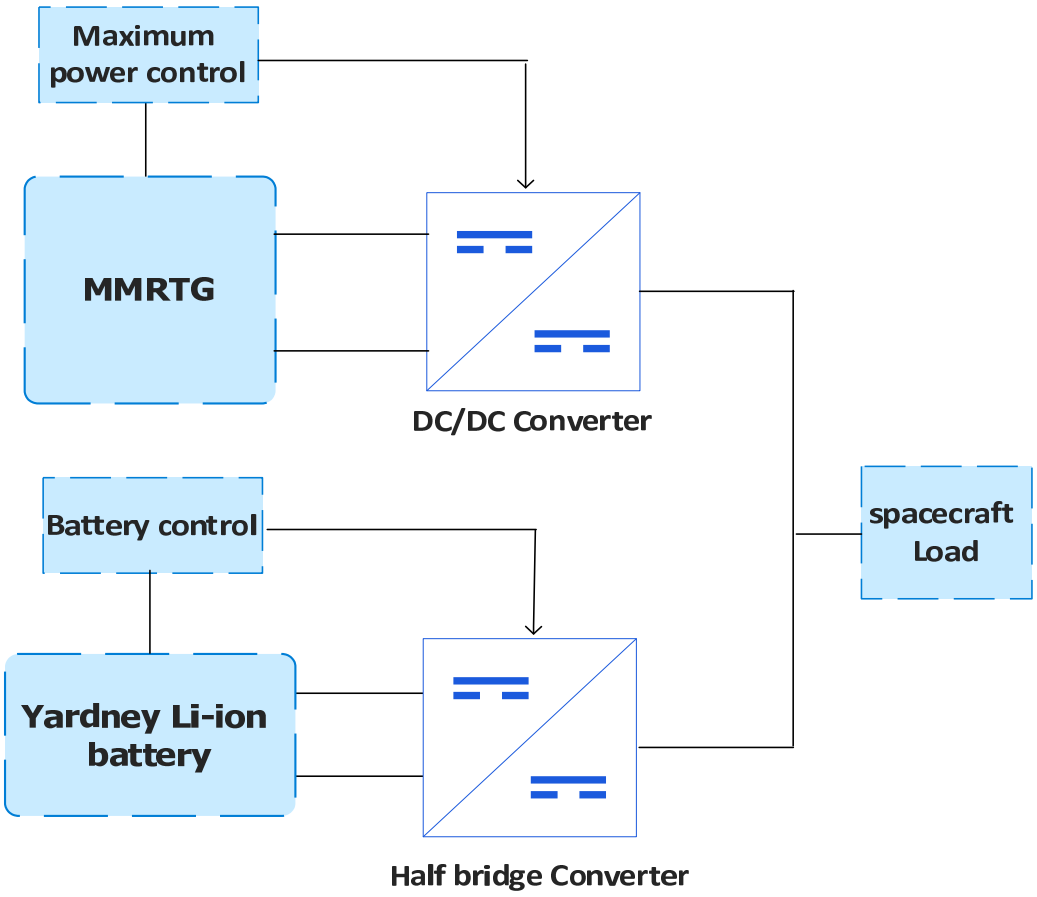

Figure 2. Hybrid energy source configuration.

2.2. Modeling of Hybrid Electrochemical-Nuclear Battery

2.2.1. Modeling of the Li-Ion Battery

The behavior of a Li-ion battery is defined by two sets of equations, given as follows [28]:

For the charging:

$$V_{batt} = E_o - K\frac{Q}{Q - it}(it + i^*) + Ae^{-Bit} - R.i \quad (1)$$

for the discharging:

$$V_{batt} = E_o - K\frac{Q}{it - 0.1Q}(i^*) - K\frac{Q}{Q - it}(it) + Ae^{-Bit} - R.i \quad (2)$$

where E_o is the constant voltage, R is the internal resistance, i is the current, K is the polarization coefficient of the electrodes, i^* is the low-frequency current dynamics, it is the extracted capacity, Q is the amount of active material in electrodes, A is the exponential voltage, and B is the exponential capacity.

MSL mission space battery LP 33450 (3.6 V; 43 Ah) was used in this investigation, and the values of relevant parameters given in Table 2 and Figure 3 illustrate the discharge characteristics of the developed Li-ion battery model at different operating temperatures.

Table 2. Battery characteristics [29].

Specifications	
Part Number	LP33450
Nominal Cell Weight	1.27 kg
Voltage Range	3.0 to 4.1 V
Nominal Voltage	3.6 V
Nominal Capacity	43 Ah at C/5 at 20 °C (68 °F)
Energy Density	378 Wh/L
Specific Energy	153 Wh/kg
Discharge Rates	Max constant current 200 A Max pulse current (< 1 s) 400 A
Nominal Cell Impedance	2 mΩ at 20 °C (68 °F)
Cycle Life (80% capacity measured at 0.5 C discharge current at 20 °C (68 °F))	>2000 at 100% DOD
Standard Charging Method	Constant current 21.5 A (0.5 C) to 4.1 V Constant voltage 4.1 V to 0.86 A (C/50)
Operating Temperature	−20 to 60 °C (−4 to 140 °F)
Storage Temperature	−40 to 60 °C (−40 to 140 °F)

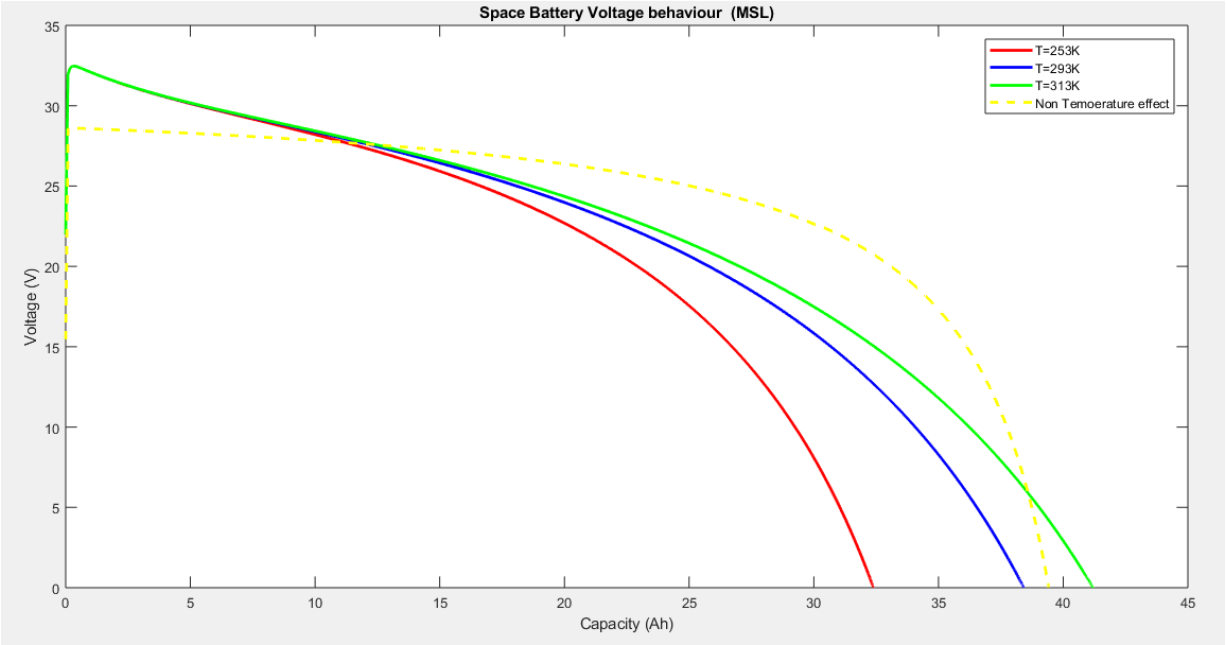

Figure 3. Li-ion battery discharge behavior.

Furthermore, the performance of a battery is affected by the temperature (either low or high) under which they operate as it affects the internal chemical reaction. At low temperatures, ionic diffusion, and migration from one electrode to the other can be difficult, causing side effects in the long term, while high-temperature operations might make the battery deliver better performance, with long-term side reactions, such as corrosion and thermal run-away. The case study of Li-ion batteries that have been found to have operating temperatures ranging from 20 °C to 60 °C are considered in this section. Jaguemont and Jow [30] established that a Li-ion battery would show signs of defect at a temperature under 10 °C. The low temperature also has effects on the State of Charge (SoC). It was found that the SoC of a Li-ion battery operating at 10 °C decreased considerably by 23% compared to a battery operating at an ambient temperature of 20 °C. The primary source of this degradation was due to the property of the electrolyte, which increases its viscosity and reduces ionic conductivity.

Low temperature resists the charge transfer, thereby adversely affecting the battery kinetics. Gao et al. [31] reported that the charge transfer resistance of a battery operating at 10 °C was twice as high as a battery operating at the ambient temperature.

In addition, low temperature affects the battery electrodes through a phenomenon known as lithium plating [32], which triggers the polarization of the anode, thereby creating residual lithium ions that are deposited on the surface of the electrodes with an overall reduction effect in the capacities of the battery [33].

On the other hand, high temperatures due to heat generation yielded improved performances. However, the exposure of batteries to high temperatures over a long period will produce a negative impact. Indeed, heat generation is a critical factor that must be understood.

Masih-Tehrani et al. [34] proposed a modified set of equations that consider the battery's temperature by making each parameter temperature dependent. Therefore, Equations (1) and (2) can be expressed as Equations (3) and (4), respectively:

$$V_{batt}(T) = E_0(T) - K(T)\frac{Q(T_a)}{Q(-it)}(it + i^*) + Ae^{-Bit} - R(T) \quad (3)$$

$$V_{batt}(T) = E_0(T) - K(T)\frac{Q(T_a)}{it - 0.1Q(T_a)}(i^*) - K(T)\frac{Q(T_a)}{Q(T_a) - it}(it) + Ae^{-Bit} - R(T).i \quad (4)$$

where

$$E_0(T) = E_0^{ref} + \frac{\partial E}{\partial T}(T - T_{ref}) \quad (5)$$

$$Q(T_a) = Q_{Ta} + \frac{\partial Q}{\partial T}(T_a - T_{ref}) \quad (6)$$

$$K(T) = K_{Tref} \times e^{[\alpha(\frac{1}{T} - \frac{1}{T_{ref}})]} \quad (7)$$

$$R(T) = R_{Tref} \times e^{[\beta(\frac{1}{T} - \frac{1}{T_{ref}})]} \quad (8)$$

R is the internal resistance,
T_{ref} is the nominal ambient temperature,
T is the cell temperature or internal temperature,
T_a is the ambient temperature,
$\frac{E}{T}$ is the reversible voltage temperature coefficient,
$\frac{\Delta Q}{\Delta T}$ is the Maximum capacity temperature coefficient,
α is the Arrhenius rate constant for polarization resistance;
β is the Arrhenius rate constant for internal resistance.

2.2.2. Modeling of MMRTG

The proposed MMRTG model is based on the work by Tsai and Lin [35] and is subject to the following assumptions:

- Steady-state radioisotope thermoelectric module (the temperature distribution of the air gap is the same as the thermoelectric elements; hence, heat transfer of the thermoelectric device can be treated as approximately one-dimensional heat transfer)
- Identical configurations of the p-type and n-type thermoelectric elements (equal lengths, widths, and thicknesses)
- Materials with a similar thermal coefficient of expansion must be chosen for the thermoelectric elements because different materials will cause a thermal expansion mismatch of the materials, which will lead to severe stress, leading to the degradation and breaking of the contacts between the thermoelectric elements (p-type and n-type semiconductors) and the ceramic substrate. Using similar materials is impossible; therefore, the thermoelectric module must be designed to minimize thermal stresses.
- Thermoelectric elements are connected electrically in series and thermally in parallel.
- The thermoelectric elements' material properties (Seebeck coefficient, thermal conductivity, and electrical conductivity) are temperature dependent.
- Uniform heat from the heat source
- Radioisotope thermoelectric module is thermal insulation packaged; hence, the heat leakage through the lateral surface is negligible.

The modeling equations of the MMRTG are as follows:
The Seebeck coefficient:

$$\begin{array}{c} S = V_{max}/T_H \\ S = 2V_m/\Delta T \end{array} \quad (9)$$

where V_{max} is the maximum voltage, V_m is the load voltage t the matched load, and $\Delta T = T_H - T_C$.

RTG manufacturers provide parameters, including the (hot temperature) T_H, (cold temperature) T_C, (matched power) W_m, (matched voltage) V_m, and (maximum efficiency) η_{max}.

The Figure of Merit:

$$\begin{array}{c} Z = S^2/R.K_{th} \\ Z = S^2/R.K_{th} \end{array} \quad (10)$$

where R is resistance, m_{opt} is the resistance ratio m that maximizes the efficiency, and K_{th} and T_{ave} are given as:

$$K_{th} = S^2/RZ \quad (11)$$

$$T_{ave} = 0.5(T_H + T_C) \quad (12)$$

The Resistance:

$$\begin{array}{c} R = V_{max}(1 - \Delta T_{max}/T_H)/I_{max} \\ R_{th} = V_{max}I_{max}(T_H - \Delta T_{max})/(2T_H\Delta T_{max}) \\ R = R_L = V_m^2/W_m \end{array} \quad (13)$$

The Current:

$$I = S\Delta T/[(1 + m)R] \quad (14)$$

where m is the resistance ratio, with the Matched load current:

$$I_m = S\Delta T/2R \quad (15)$$

The Thermal efficiency:

$$\eta_{th} = I^2R_L/Q_H \quad (16)$$

where Q_H is the thermal power input to the hot side.

The Max Thermal efficiency:

$$\eta_{th}^{max} = (m_{opt} - 1)(\Delta T / T_H) / (m_{opt} + T_C / T_H) \quad (17)$$

the Matched load efficiency:

$$\eta_{th.m} = Z\Delta T / [4 + Z(1.5\, T_H + 0.5 T_C) \quad (18)$$

the optimal resistance ratio:

$$\begin{gathered} m_{opt} = (1 + ZT_{ave})^{0.5} \\ m_{opt} = (\Delta T + \eta_{th}^{max} T_C) / (\Delta T - \eta_{th}^{max} T_H) \end{gathered} \quad (19)$$

where η_{th}^{max} is the maximal efficiency.

The Short circuit current:

$$I_{SC} = 2I_m = 2W_m / V_m. \quad (20)$$

The modeling parameters for the typical MMRTG used in the 2011 Mars Science Laboratory mission and other used parameter values are given in Table 3.

Table 3. MMRTG modeling equations and parameter values [36].

Design Parameters	**MMRTG**
No. of GPHS bricks	8
TE materials	PbTe(TAGS 85, PbSnTe)
No. of couples	768
Design-point QHS	1984 WTh @ BOL
TE hot-side temp	525 °C
TE cold-side temp	100–200 °C
BOL power (WE)	~120
Est. EOL (14 years) power	60
BOL system efficiency	6.0%
Specific power (WE kg^{-1})	2.8
Containment system	Argon overpressure
Mission usage	Multi-mission
Addressed program	MSL and Mars 2020
Parameter	Value
Efficiency (thermal to electrical conversion)	6.3%
Thermal power	2000 W
Electrical power	110 W
Specific power	2.8 We/Kg
Output voltage	28–32 V dc
Hot-side temperature	525 °C
Cold-side temperature	100–200 °C
Figure of merit, Z	0.001032 Z^{-1}
Seebeck coefficient, S	0.1818 V/K
Thermal conductivity, Kth	4.271 W/K
Resistance, R	7.5 Ω

To validate the developed MMRTG model, a simulation was carried out using the Matlab/Simulink tool, and Figure 4 depicts the MMRTG voltage versus current (Figure 4a) and the power versus current (Figure 4b). It can be observed that the maximum efficiency of 6.3% was achieved when the current was 4.2 A.

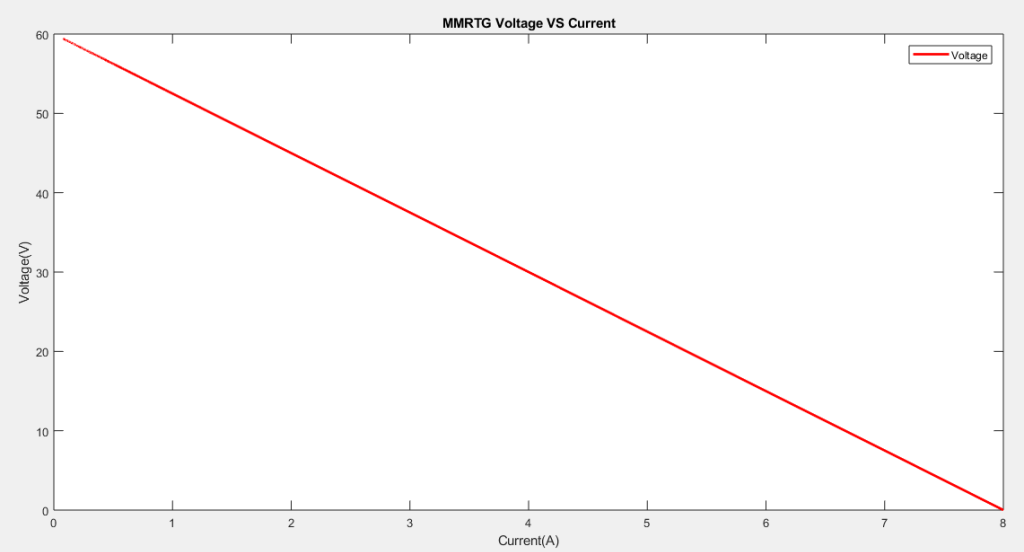

(**a**)

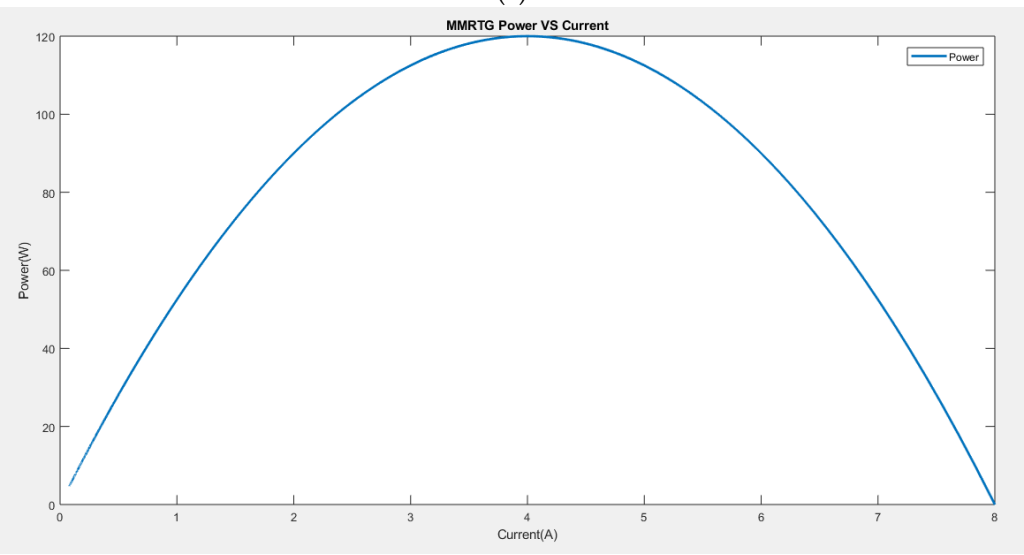

(**b**)

Figure 4. (**a**) Voltage versus current and (**b**) power versus current of the modeled MMRTG.

2.2.3. Modeling of Auxiliary Components

The auxiliary components included the boost converter, half-bridge converter, and the DC electric motor serving as the load. The parameters of the DC motor are given in Table 4 and the design features of the boost and half-bridge converters are provided in Table 5.

Table 4. Motor parameters [37].

Description	Value
Armature resistance R_a (Ω)	1
Armature inductance L_a (H)	0.5
Torque constant K_t	0.01
Moment of inertia J (Kg m^2 S^{-2})	0.01
EMF constant	0.01
Friction coefficient B	0.1

Table 5. Power converters designed parameters.

Boost Converter	
Description	**Value**
MMRTE voltage (V)	34.25
Motor voltage (V)	60
Switching frequency (kHz)	25
Voltage ripple	1%
Minimum inductance (μH)	7
Minimum capacitor (mF)	1.72
Duty cycle	43%
Half-bridge converter	
Battery voltage (V)	30
Duty cycle	57%
Minimum inductance (μH)	15
Load capacitor (mF)	5
Minimum battery capacitor (mF)	2.3

3. Results and Discussion

The hybrid energy system, depicted in Figure 2, was modeled and simulated for a duration of 8 h and the simulation results are shown in Figures 5–7. It can be seen that the voltage of the Li-ion battery was constantly around 34 V, while that of the MMRTG occurred between 17 and 39 V. The output voltage of the hybrid energy system, on the other hand, reached a maximum value of 60 V, when the battery voltage discharges. However, when the output voltage dropped to 40 V, it was due to increased battery voltage during charging (Figure 5a). Therefore, the system, if subjected to appropriate development and the right conditions, is capable of power leveling (supply additional power), battery charging, and recovery mode.

Figure 5b shows that the current through the motor increases considerably during battery discharge and decreases when the battery charges. It could be seen that the current ripples are unstable. Thus, the system might operate at a high-power demand but only for a limited time. It can be observed that during the transient regime, the initial current is zero when the motor is connected to the output terminals of the boost converter, and it takes some time for it to attain the nominal current because of the inductance in the armature circuit. The motor reaches its steady state once the current settles around 47 A, which is its final value. However, this current is subjected to ripples, making the final value of the current oscillate between 45 and 50 A. These ripples originate from the boost converter's output as the motor receives its supply. When the converter's inductor stores energy, the output voltage decreases and rises when the energy is released.

Figure 5c shows the output power of the Li-ion battery, the MMRTG, and the hybrid energy system. The results show that the MMRTG power was around 110 W, while the Li-ion battery power varies between 3500 W and −2500 W during charging and discharging. The rather unstable power behavior from the battery does not affect the power stability of the motor. Thus, the arrangement of the hybrid system provides a viable and relatively stable power at its output, regardless of the input power behavior.

The above hybrid system, however, can be compared to the result obtained from a single supply RTG connected to the motor (Figure 6). The comparison in Figure 6a shows that the voltage of 48 V boosted from the RTG single system was inferior to the voltage delivered by the hybrid system when charged by a 60 V battery.

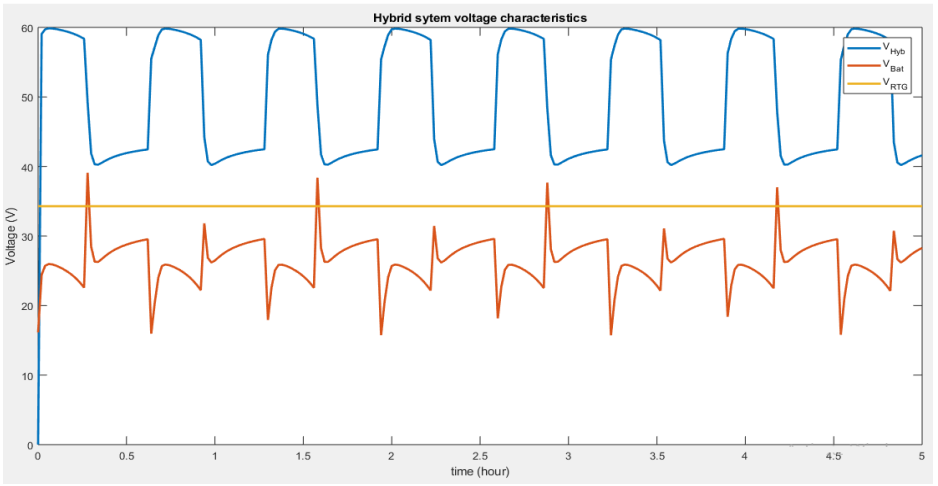

(**a**)

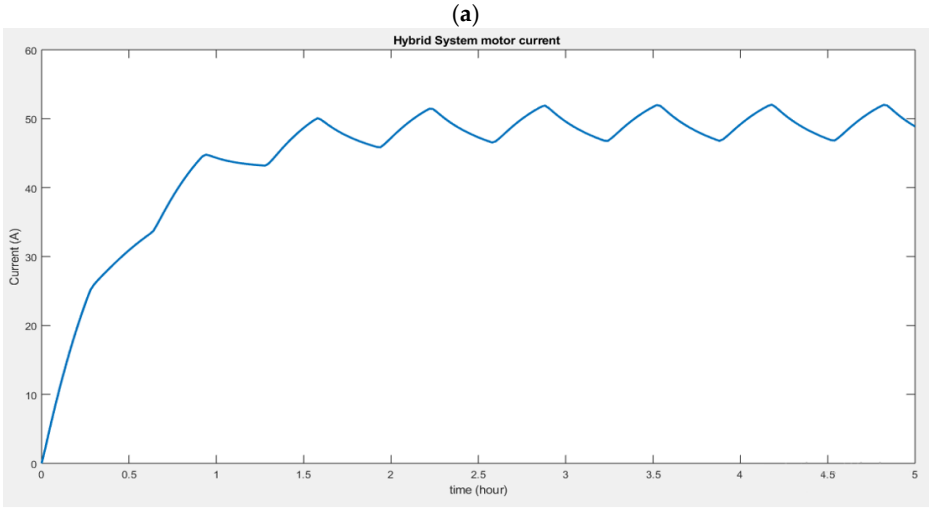

(**b**)

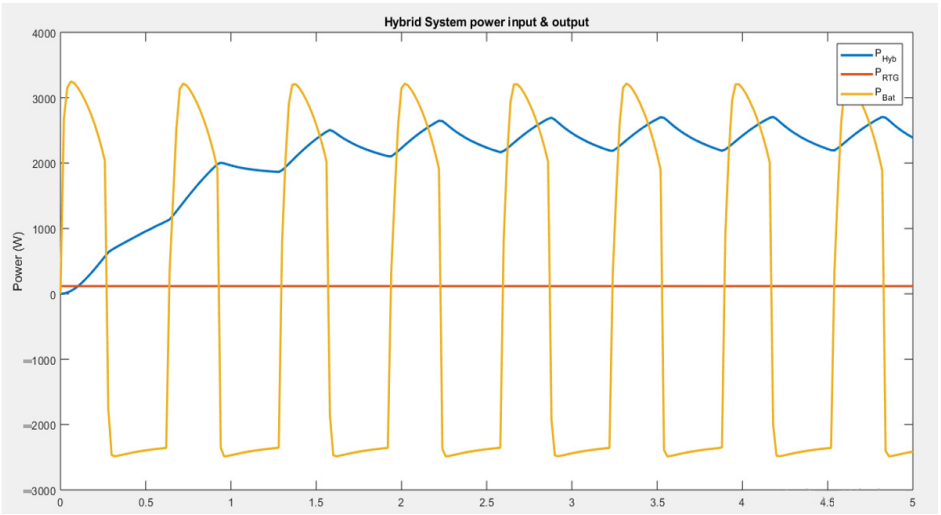

(**c**)

Figure 5. (**a**) Output voltage, (**b**) load current, and (**c**) input and output power of the hybrid battery.

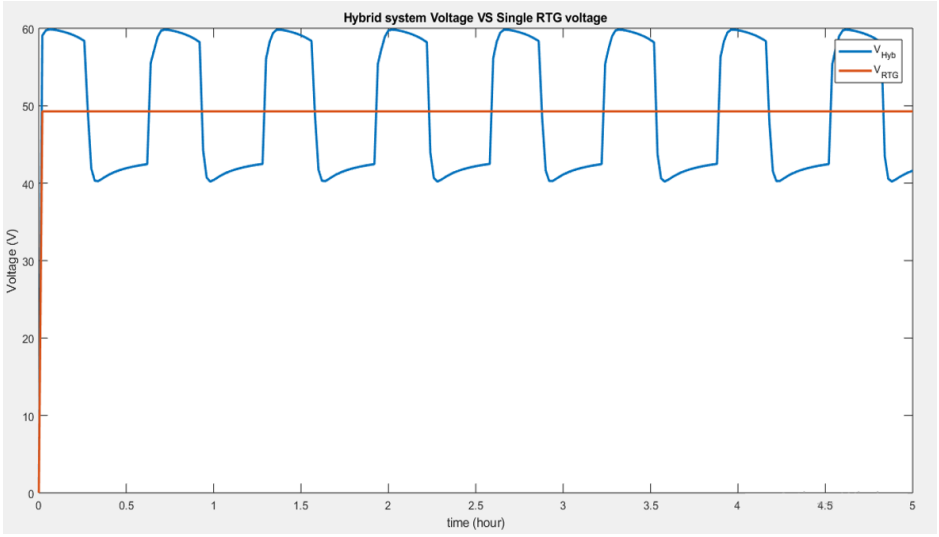

(**a**)

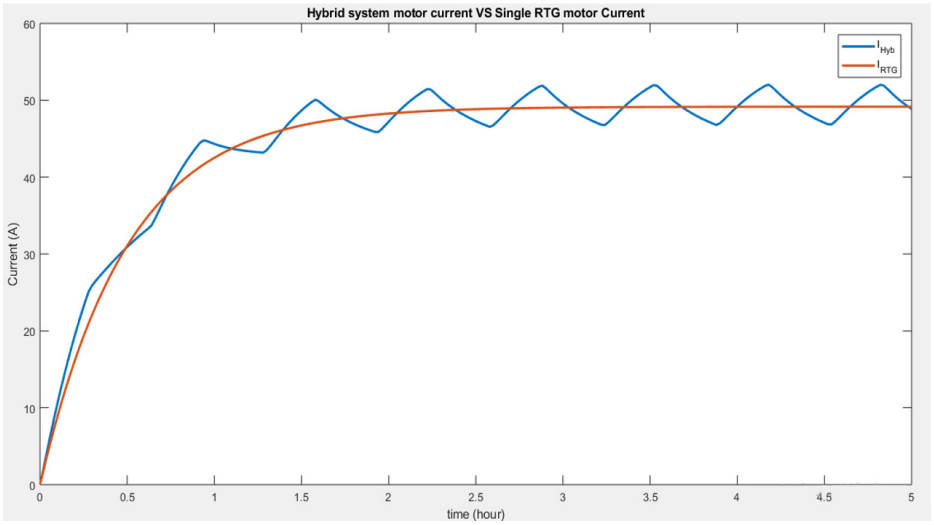

(**b**)

Figure 6. (**a**) Hybrid voltage vs. RTG voltage, and (**b**) hybrid current vs. RTG current.

Figure 6b suggests that the current through the motor is higher when connected to the hybrid system than when powered by a single RTG.

Therefore, the hybrid system can deliver better performances when additional power is needed, recharging the battery when necessary, and it can also solely rely on the MMRTG power, making it more advantageous.

The voltage plot presented in Figure 7a shows that the load voltage tends to be superior at a higher resistance; indeed, the hybrid system exhibits the highest output voltage of 95 V when a load of 7 Ω is connected; meanwhile, the smallest load of 1 Ω only provides a voltage of 60 V during discharge. It is also interesting to see that the higher load tends to increase the battery discharge life, at about half an hour (30 min) up to an hour, when operated at 1 Ω and 7 Ω, respectively. Moreover, it could be observed that even after the battery-fed discharge voltage period has flattened out, the constant voltage out of the hybrid system is only the voltage produced by the boost converter coming from the RTG. In contrast, Figure 7b shows that the current through the 1 Ω resistance is at its highest during discharge. Meanwhile, this 7 Ω resistor shows the smallest amount of current.

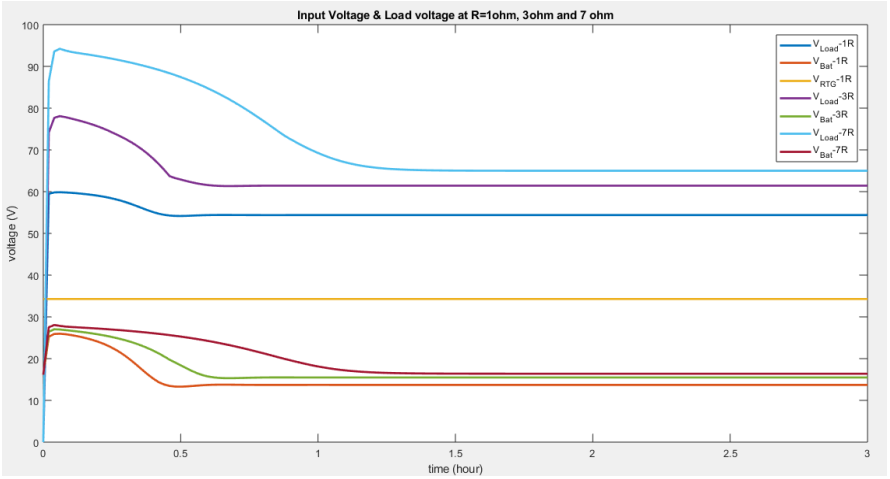

(**a**)

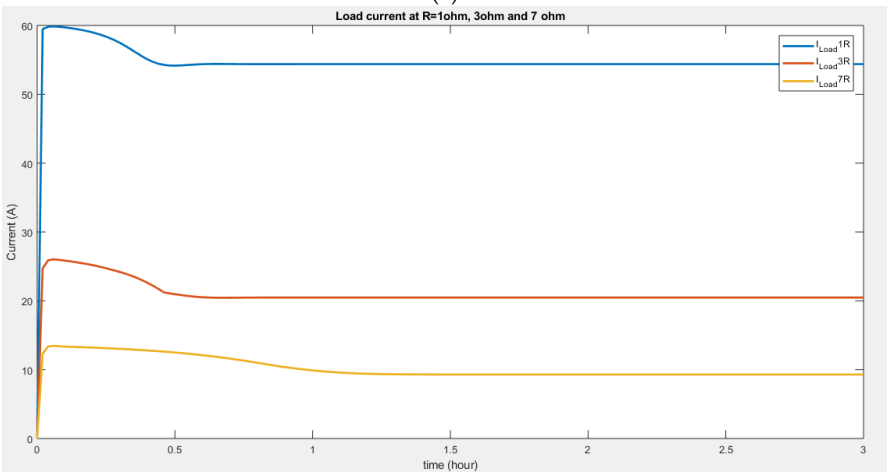

(**b**)

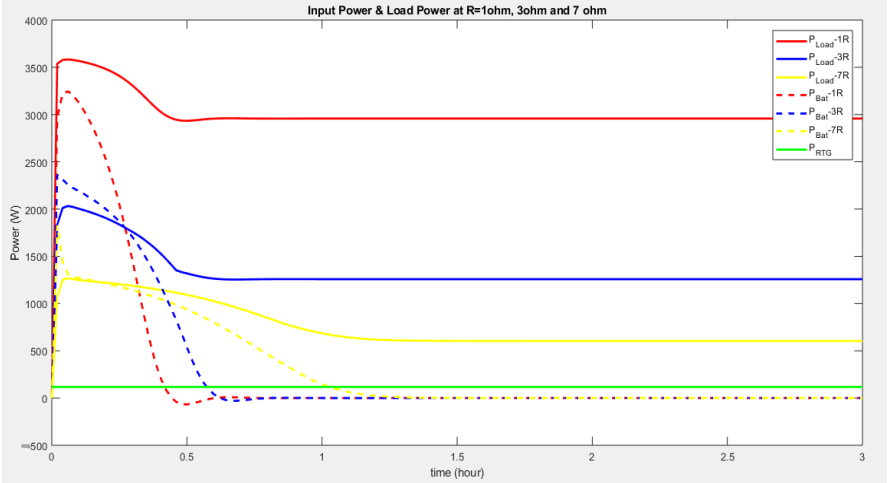

(**c**)

Figure 7. (**a**) Voltage characteristics under different resistance values, (**b**) load current under different resistance values, and (**c**) power input versus power output at different load resistances.

Figure 7c shows that the highest peak of power is obtained at the lowest load resistance of 1 Ω at 3500 W, followed by the mid-range resistance of 3 Ω at 2000 W, and the highest resistance of 7 Ω at 1250 W. It could also be seen that the peak in power comes entirely from the battery power, which turned out to be superior to the output power only in the 1 Ω load, while in other types of loads, the output power is lower than the battery. It is evident that the peak in power takes a considerable time to fade during the discharge

period, regarding the amount of resistance R; indeed, the more resistance, the longer the power being supplied to the load remained at its peak. The result of the test conducted by varying the load resistance shows that the lower the resistance, the better the power at the output. Even though it has the inconvenience of operating at peaks for a shorter period, the shorter operating time was only a minor issue since the battery was recharged during its operation and was required to be used for maximum power delivery.

Figure 8a,b show the charge and discharge cycles of the batteries, respectively, at three different ambient temperatures (253 °K, 293 °K, and 313 °K). It is evident that throughout the 5 h operations, the battery tended to charge and discharge more often at the lower temperature (253 °K) than at the higher temperature (293 °K). This is because the charge delivered by the battery at a low temperature is poor. Consequently, more charge–discharge was needed to compensate for the load of the hybrid system. The hybrid battery system operated optimally at a higher temperature.

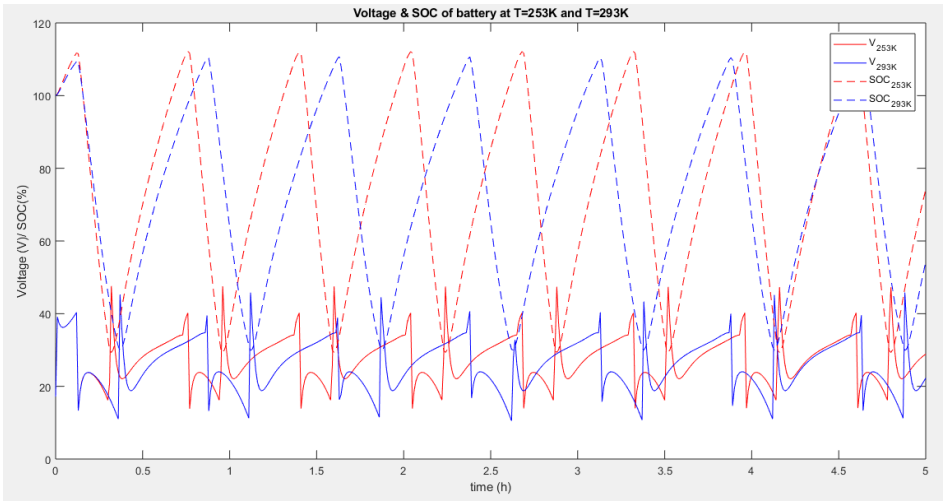

(**a**)

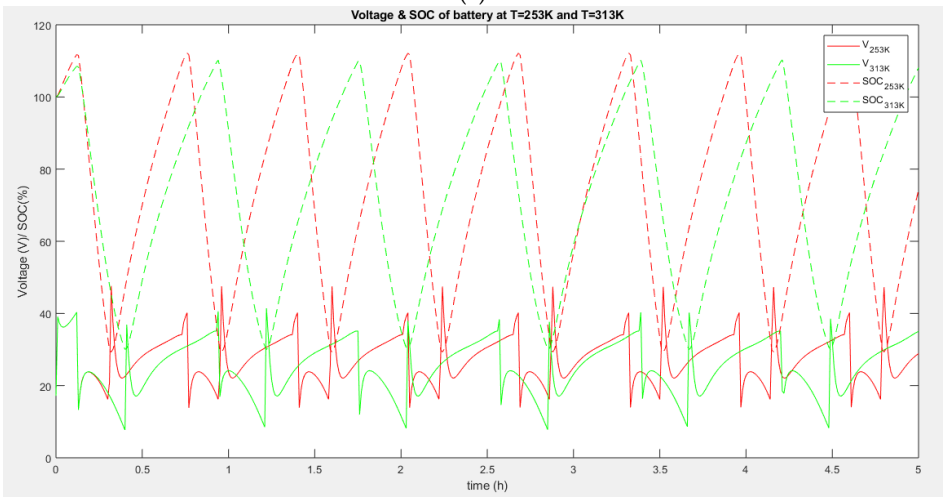

(**b**)

Figure 8. Performances of hybrid batteries at (**a**) 253 °K and 293 °K, and (**b**) at 253 °K and 313 °K.

Additionally, the assessment showed that at the same temperature, the output voltage of the hybrid battery was higher than the single battery; however, it is interesting to note that a change in temperature did not affect the output voltages of the hybrid battery. It could be seen that the hybrid system output voltage at temperature T = 253 °K and the hybrid system output voltage at T = 293 °K are relatively equal. However, it could be observed that the power cycle (when the hybrid voltage was at its maximum) is wider and takes a long time before dropping. Moreover, the number of charge–discharge cycles was

less at higher temperatures compared to low temperatures. Indeed, the charge–discharge cycle refers to charging a battery and discharging it into a load. Charge–discharge cycles are also used to describe the lifespan of a battery. Since all chemical reactions are affected by temperature and because batteries rely on chemical reactions to generate power, the change in temperature affects the battery power. Batteries operate best at room temperature. A battery's capacity and expected life can fluctuate with a small temperature change. Therefore, because of the reduced internal resistance and increased chemical metabolism, the capacity of the battery rises as the temperature rises. However, if such conditions persist for a long duration, the expected life of the battery shortens.

These results should not be overlooked in the design of an appropriate battery management system. Overall, while the performance of the battery improves as the temperature increases, it should be noted that prolonged exposure to high temperatures could shorten the lifespan of the battery.

4. Conclusions

This research evaluated the modeling of a hybrid multi-mission radioisotope thermoelectric generator (MMRTG)-lithium-ion (Li-ion) battery integrated energy storage system for spacecraft applications in order to combine the RTGs' long lifespan and reliability benefits with the rechargeability and high energy density of the Li-ion battery to achieve a single energy unit. The primary goal of the study was to develop a power unit that could overcome the constraints of MMRTG and Li-ion batteries to produce a highly efficient and reliable power source for spacecraft applications. A 110 W/32 V RTG and a 3.6 V/43 Ah Li-ion battery were coupled to a DC motor through power converters in the proposed hybrid system. The modeling and simulation were performed using MATLAB/Simulink. The results show that the hybrid energy system can potentially improve the efficiency, reliability, and duration of a spacecraft's mission. The hybrid energy system was assessed under different load conditions, and it was observed that the hybrid system exhibited the highest output voltage of 95 V when a load of 7 Ω was connected to it. It was also noticed that a higher load tended to increase the discharge life of the battery, from about half an hour (30 min) to an hour, when operated at 1 Ω and 7 Ω, respectively.

On the other hand, the power assessment revealed that the highest power peak was achieved at a load resistance of 1 Ω at 3500 W. Furthermore, since batteries are required to operate in a constantly changing environment, the effects of temperatures on batteries were investigated. The results show that the hybrid energy system output voltage at a temperature of T = 253 °K and an output voltage of T = 293 °K were relatively equal. However, it could be observed that the power cycle (when the hybrid voltage is at maximum) was wider and required a long time before dropping. Furthermore, the number of charge–discharge cycles was less at high temperatures than at low temperatures. Further study should investigate the hybrid energy system's long-term behavior, including its performance degradation, aging effects, reliability assessments, and the possibility of replacing the Li-ion battery with a semiconductor material.

Author Contributions: Conceptualization, O.L.A.; methodology, O.L.A.; software, O.L.A.; validation, O.L.A.; formal analysis, O.L.A.; investigation, O.L.A.; writing—original draft preparation, O.L.A. and D.N.L.; writing—review and editing, O.L.A. and D.N.L.; supervision, M.T.K.; All authors have read and agreed to the published version of the manuscript.

Funding: This research received no external funding.

Institutional Review Board Statement: Not applicable.

Informed Consent Statement: Not applicable.

Data Availability Statement: Not applicable.

Conflicts of Interest: The authors declare no conflict of interest.

References

1. Fakham, H.; Lu, D.; Francois, B. Power Control Design of a Battery Charger in a Hybrid Active PV Generator for Load-Following Applications. *IEEE Trans. Ind. Electron.* **2011**, *58*, 85–94. [CrossRef]
2. Becherif, M. *Passivity-Based Control of Hybrid Sources: Fuel Cell and Battery*; IFAC: Geneva, Switzerland, 2006; Volume 11, ISBN 9783902661135.
3. Ambrosi, R.M.; Williams, H.; Watkinson, E.J.; Barco, A.; Mesalam, R.; Crawford, T.; Bicknell, C.; Samara-Ratna, P.; Vernon, D.; Bannister, N.; et al. European Radioisotope Thermoelectric Generators (RTGs) and Radioisotope Heater Units (RHUs) for Space Science and Exploration. *Space Sci. Rev.* **2019**, *215*, 55. [CrossRef]
4. Obodovskiy, I. Atomic Energy Sources. In *Radiation: Fundamentals, Applications, Risks, and Safety*; Elsevier: Amsterdam, The Netherlands, 2019; pp. 361–365. ISBN 9780444639790.
5. Zoui, M.A.; Bentouba, S.; Stocholm, J.G.; Bourouis, M. A Review on Thermoelectric Generators: Progress and Applications. *Energies* **2020**, *13*, 3606. [CrossRef]
6. Abd El-Hameed, A.M. Radiation Effects on Composite Materials Used in Space Systems: A Review. *NRIAG J. Astron. Geophys.* **2022**, *11*, 313–324. [CrossRef]
7. Azeem, M.M.; Wang, Q.; Li, Z.; Zhang, Y. Dislocation-Oxide Interaction in Y_2O_3 Embedded Fe: A Molecular Dynamics Simulation Study. *Nucl. Eng. Technol.* **2020**, *52*, 337–343. [CrossRef]
8. Mustafa Azeem, M.; Li, Z.; Wang, Q.; Zubair, M. Molecular Dynamics Studies and Irradiation Effects in ODSS Alloys. *Int. J. Nucl. Energy Sci. Technol.* **2018**, *12*, 381–399. [CrossRef]
9. NASA Radioisotope Thermoelectric Generator. Space Radioisotope Power Systems. Available online: https://science.nasa.gov/about-us/smd-programs/radioisotope-power-systems#:~:text=TheRadioisotopePowerSystems(RPS,enablefuturespaceexplorationmissions (accessed on 16 June 2015).
10. Chou, S.K.; Yang, W.M.; Chua, K.J.; Li, J.; Zhang, K.L. Development of Micro Power Generators—A Review. *Appl. Energy* **2011**, *88*, 1–16. [CrossRef]
11. Ghamaty, S.; Bass, J.C.; Elsner, N.B. Quantum Well Thermoelectric Devices and Applications. In Proceedings of the 22nd International Conference on Thermoelectrics, ICT, La Grande Motte, France, 17–21 August 2003; pp. 563–566.
12. Gulian, A.; Wood, K.; Fritz, G.; Gyulamiryan, A.; Nikogosyan, V.; Giordano, N.; Jacobs, T.; Van Vechten, D. X-Ray/UV Single Photon Detectors with Isotropic Seebeck Sensors. *Nucl. Instrum. Methods Phys. Res. Sect. A Accel. Spectrometers Detect. Assoc. Equip.* **2000**, *444*, 232–236. [CrossRef]
13. NASA. General Purpose Heat Source | Thermal Systems—NASA RPS: Radioisotope Power Systems. Available online: https://rps.nasa.gov/power-and-thermal-systems/thermal-systems/general-purpose-heat-source/ (accessed on 15 April 2023).
14. NASA. Multi-Mission Radioisotope Thermoelectric Generator (MMRTG). Available online: https://mars.nasa.gov/internal_resources/788/ (accessed on 10 April 2023).
15. Jouhara, H.; Żabnieńska-Góra, A.; Khordehgah, N.; Doraghi, Q.; Ahmad, L.; Norman, L.; Axcell, B.; Wrobel, L.; Dai, S. Thermoelectric Generator (TEG) Technologies and Applications. *Int. J. Thermofluids* **2021**, *9*, 100063. [CrossRef]
16. Sethumadhavan, S.; Burger, D. Powering a Cat Warmer Using Bi_2Te_3 Thin-Film Thermoelectric Conversion of Microprocessor Waste Heat. In Proceedings of the ASPLOS, San Jose, CA, USA, 21–25 October 2006.
17. Rowe, D.M. Thermoelectrics, an Environmentally-Friendly Source of Electrical Power. *Renew. Energy* **1999**, *16*, 1251–1256. [CrossRef]
18. Jaziri, N.; Boughamoura, A.; Müller, J.; Mezghani, B.; Tounsi, F.; Ismail, M. A Comprehensive Review of Thermoelectric Generators: Technologies and Common Applications. *Energy Rep.* **2020**, *6*, 264–287. [CrossRef]
19. Streb, A.J. *Radioisotope Power Systems for Manned Space Stations*; Academic Press Inc.: Cambridge, MA, USA, 1966; Volume 16.
20. Ragheb, M. Radioisotopes Power Production. Available online: https://mragheb.com/NPRE402ME405NuclearPowerEngineering/RadioisotopesPowerProduction.pdf (accessed on 13 April 2023).
21. Riaz, A.; Sarker, M.R.; Saad, M.H.M.; Mohamed, R. Review on Comparison of Different Energy Storage Technologies Used in Micro-Energy Harvesting, Wsns, Low-Cost Microelectronic Devices: Challenges and Recommendations. *Sensors* **2021**, *21*, 5041. [CrossRef]
22. Marsh, R.A.; Vukson, S.; Surampudi, S.; Ratnakumar, B.V.; Smart, M.C.; Manzo, M.; Dalton, P.J. Li Ion Batteries for Aerospace Applications. *J. Power Sources* **2001**, *97–98*, 25–27. [CrossRef]
23. Ratnakumar, B.V.; Smart, M.C.; Ewell, R.C.; Whitcanack, L.D.; Chin, K.B.; Surampudi, S. Lithium-Ion Rechargeable Batteries on Mars Rovers. In Proceedings of the 2nd International Energy Conversion Engineering Conference, Providence, RI, USA, 16–19 August 2004; Volume 3, pp. 1763–1770.
24. NASA. JPL | Electrochemical Technology—Mission Support. Available online: https://electrochem.jpl.nasa.gov/?page=mission-support (accessed on 15 April 2023).
25. Miao, Y.; Hynan, P.; Von Jouanne, A.; Yokochi, A. Current Li-Ion Battery Technologies in Electric Vehicles and Opportunities for Advancements. *Energies* **2019**, *12*, 1074. [CrossRef]
26. Ratnakumar, B.V.; Smart, M.C.; Kindler, A.; Frank, H.; Ewell, R.; Surampudi, S. Lithium Batteries for Aerospace Applications: 2003 Mars Exploration Rover. *J. Power Sources* **2003**, *119–121*, 906–910. [CrossRef]
27. Clean Energy Institute Lithium-Ion Battery | Clean Energy Institute. Available online: https://www.cei.washington.edu/education/science-of-solar/battery-technology/ (accessed on 18 May 2023).

28. Shepherd, C.M. Design of Primary and Secondary Cells. *J. Electrochem. Soc.* **1965**, *112*, 657. [CrossRef]
29. SATNOW LP 33450—EaglePicher Technologies | Satellite Battery. Available online: https://www.satnow.com/products/batteries/eaglepicher-technologies/98-1276-lp-33450 (accessed on 25 April 2023).
30. Jaguemont, J.; Boulon, L.; Dubé, Y. A Comprehensive Review of Lithium-Ion Batteries Used in Hybrid and Electric Vehicles at Cold Temperatures. *Appl. Energy* **2016**, *164*, 99–114. [CrossRef]
31. Gao, F.; Tang, Z. Kinetic Behavior of LiFePO4/C Cathode Material for Lithium-Ion Batteries. *Electrochim. Acta* **2008**, *53*, 5071–5075. [CrossRef]
32. Petzl, M.; Kasper, M.; Danzer, M.A. Lithium Plating in a Commercial Lithium-Ion Battery—A Low-Temperature Aging Study. *J. Power Sources* **2015**, *275*, 799–807. [CrossRef]
33. Gunawardhana, N.; Dimov, N.; Sasidharan, M.; Park, G.J.; Nakamura, H.; Yoshio, M. Suppression of Lithium Deposition at Sub-Zero Temperatures on Graphite by Surface Modification. *Electrochem. Commun.* **2011**, *13*, 1116–1118. [CrossRef]
34. Masih-Tehrani, M.; Yahyaei, R. Study of Lithium Battery Thermal Effect on Battery and Hybrid Battery/Ultra-Capacitor Sizing for an Electric Vehicle. *J. Eng. Technol.* **2017**, *6*, 85–99.
35. Tsai, H.L.; Lin, J.M. Model Building and Simulation of Thermoelectric Module Using Matlab/Simulink. *J. Electron. Mater.* **2010**, *39*, 2105–2111. [CrossRef]
36. Holgate, T.C.; Bennett, R.; Hammel, T.; Caillat, T.; Keyser, S.; Sievers, B. Increasing the Efficiency of the Multi-Mission Radioisotope Thermoelectric Generator. *J. Electron. Mater.* **2015**, *44*, 1814–1821. [CrossRef]
37. Kushwah, M.; Patra, A. PID Controller Tuning Using Ziegler-Nichols Method for Speed Control of DC Motor. *Int. J. Sci. Eng. Technol. Res.* **2014**, *3*, 2924–2929.